Hydrodeoxygenation of aqueous phase catalytic pyrolysis oil to liquid hydrocarbons using multi-functional nickel catalyst

Hossein Jahromi [*], Foster A. Agblevor

USTAR Bioenergy Center, Department of Biological Engineering, Utah State University, UT 84322, USA

---

* Corresponding author email address: hossein.jahromi@aggiemail.usu.edu

Abstract

Herein we investigated the hydrodeoxygenation (HDO) of aqueous phase pinyon-juniper catalytic pyrolysis oil (APPJCPO) using a new multifunctional red mud-supported nickel (Ni/RM) catalyst. The organic liquid yield after HDO of APPJCPO using 30 wt. % Ni/RM at reaction temperature of 350 °C was 47.8 wt. % with oxygen content of 1.14 wt. %. The organic liquid fraction consisted of aliphatics, aromatics, and alkylated aromatic hydrocarbons as well as small amounts of oxygenates. The RM support catalyzed ketonization of carboxylic acids. The Ni metal catalyzed partial reduction of oxygenates that underwent carbonyl alkylation with aldehydes and ketones on the RM. Catalyst deactivation assessment suggested that oxidation and coke formation were the main controlling factors for deactivation of Ni and RM respectively. For comparison, commercial (~65wt.%) Ni/SiO_2-Al_2O_3 was tested in HDO experiments which gasified the soluble organics in APPJCPO and did not produce liquid hydrocarbons.

Keywords:

Hydrodeoxygenation, pyrolysis, red mud, nickel catalysts, catalyst deactivation, bio-oils

1. Introduction

Lignocellulosic biomass is the most abundant renewable source of organic carbon on earth and the only one of low enough cost and adequate availability for large scale sustainable production of liquid fuels. Lignocellulosic biomass can be thermochemically converted into transportation fuels through three intermediate major pathways: gasification for syngas, pyrolysis or liquefaction for bio-oils, and hydrolysis of biomass to produce sugar monomer units.[1, 2] Pyrolysis is a thermal decomposition of organic compounds in the absence of oxidizing agents. This process produces char, gas, and liquid products. The liquid product (bio-oil) can be upgraded to transportation fuel through various processes including catalytic cracking, hydrodeoxygenation (HDO), emulsification, esterification with supercritical ethanol, and steam reforming followed by Fischer Tropsch synthesis.[2, 3] The aqueous fraction of pyrolysis oil contains about 10~30% soluble organics such as aldehydes, ketones, acids, and phenolics.[4, 5] The water-soluble organics can potentially cause corrosion of processing equipment, require wastewater treatment, and a potential source of carbon loss for the biomass conversion processes.

Low-temperature hydrogenation of the water-soluble portion of bio-oil, and reforming (to H_2) or dehydration/hydrogenation (to C_1−C_6 alkanes) are some of the methods used in processing aqueous fraction of bio-oils.[6] The hydrogenation process improves its thermal stability for further upgrading processes. Vispute and Huber showed that 15% of the carbon is lost in the solid and gas products during hydrogenation of bio-oil at 125 °C and that levoglucosan, sugars and aromatic rings were not fully converted to the corresponding alcohols at 125 °C.[7] Further, Li et al. converted an aqueous carbohydrate stream from maple wood into gasoline range products with carbon yield of 57% in a 2-step aqueous phase processing over Ru/C catalyst (1st step) and Pt/ZrP catalyst (2nd step).[8] Other catalysts such as dolomite and WO_3/ZrO_2 have also been investigated for stabilization

and upgrading of bio-oil and showed promise.[8-10] These studies showed that the challenge with hydrogenation of water-soluble fraction of bio-oil is to minimize the H_2 consumption and carbon loss, while achieving high selectivity of the desired products. The current bio-oil HDO state of the art indicates that there is a wide range of products formed and that the associated catalytic chemistry needs to be understood in more detail.[7-11]

The structure of three major polymeric components, cellulose, hemicellulose, and lignin, are well-represented by the bio-oil components in the case of lignocellulosic biomass-derived pyrolysis oil. HDO is usually the preferred method among upgrading processes since it can produce high quality fuels. HDO can improve pyrolysis oil quality through improving oil stability and higher energy density.[12] HDO of the bio-oil involves four major classes of reactions (1) hydrogenation of C–O, C=O, and C=C bonds, (2) dehydration of C–OH groups, (3) C–C bond cleavage by retro-aldol condensation and decarbonylation, and (4) hydrogenolysis of C–O–C bonds.[1, 13, 14] In most HDO studies, guaiacol (representing the large number of mono- and dimethoxy phenols),[15-17] furfural (representing a major pyrolysis product group from cellulosics),[18-22] and acetic acid (representing a major product from hemicellulose)[23-25] have been studied as model compounds of bio-oil.[26, 27] These studies indicated that catalyst deactivation is a major challenge during HDO of bio-oil. One of the catalyst deactivation mechanisms that occur during HDO of bio-oil is carbon deposition on the catalyst surface. This deactivation represents a major limit of this technology because the catalyst has to be frequently regenerated. One approach that has been reported is to develop HDO catalysts that have low acidity and hence a lower rate of coke formation.[1, 13] The synthesis of an efficient catalyst can play a crucial role in HDO process.[28]

Red mud (RM), or bauxite residue, a reddish-brown strongly alkaline solid waste, is the by-product of alumina production using the Bayer process. RM contains a diverse mixture of metal

oxides, including Fe, Al, Ti, Na, Ca, and Si, as well as some trace elements, including Ga, Cr, Mn, Ni, S, Zr, K, and Co, but the actual composition depends on the process origin.[29-34] Although red mud has been investigated as a catalyst,[35-38] environmental remediation,[39] ceramics, building materials,[40] fillers, sorbents and coagulants,[41] and valuable metals recovery;[42] it is still disposed in clay-lined dams or dykes and allowed to dry naturally.

In this work, we synthesized Ni catalysts supported on RM (Ni/RM) and compared their performance with that of commercial Ni/SiO_2-Al_2O_3 in HDO of aqueous phase pinyon-juniper catalytic pyrolysis oil (APPJCPO) to produce hydrocarbons.

2. Materials and methods

2.1. Material

Pinyon-juniper (PJ) biomass chips were provided by the U.S. Bureau of Land Management. Red mud (RM) was used as catalyst for fast pyrolysis of biomass. The wet red mud was dried at room temperature, reformulated and then ground and sieved to a particle size of 125−180 μm. The ground particles were calcined at 550 °C in a muffle furnace (Thermo Fisher Scientific, Waltham, MA) for 5 h before being used for the pyrolysis. The detailed characterization of the red mud has been reported by Yathavan and Agblevor.[35] Nickel on silica-alumina (~65 wt % loading Ni) catalyst powder was obtained from Sigma-Aldrich (St. Louis, MO, USA). High purity (99%) hydrogen (Airgas, Radnor, PA, USA) was used for HDO experiments.

2.2. Pyrolysis of biomass

PJ wood chips ground to pass a 2-mm mesh were used as feedstock for production of catalytic pyrolysis oil. The pyrolysis was carried out in a pilot plant bubbling fluidized bed reactor

described in detail by Mante and Agblevor.[40] At feeding rate of 0.9 kg/h (2 lb/h), catalytic pyrolysis oil was produced at 400 ° C using RM catalyst. The pyrolytic products were condensed using a series of two ethylene glycol-cooled condensers and an electrostatic precipitator (ESP) operating at 30 kV. The ESP oil contained only about 3 wt. % water while the condenser liquids contain 60 wt. % water. Details of the pyrolysis pilot plant can be found elsewhere.[43] Liquid products captured by condensers were collected in centrifuge test tubes and centrifuged for 30 minutes at g-force of 2147 to separate the aqueous phase from the insoluble heavy oils. The aqueous phase was used for HDO experiments in this study.

2.3. Characterization of APPJCPO

The water content of APPJCPO was determined by Karl-Fisher titration method with Hydranal® -composite 5 solution. A Metrohm 701KF Titrino and 703 titration stand setup (Brinkmann Instruments, Riverview, FL) were used for the volumetric Karl Fischer titration. The pH was measured using Mettler Toledo pH Meter and probe (Mettler Toledo GmbH, Switzerland). The elemental composition of APPJCPO was determined using ThermoFischer Scientific Flash 2000 organic elemental analyzer (ThermoFisher Scientific,Waltham, MA), and the oxygen content was calculated by difference according to ASTM D5291. The GC-MS analysis of the APPJCPO was conducted by Pacific Northwest National Laboratory (PNNL) (Richland, WA, USA).

2.4. Ni/RM catalysts preparation and characterization

Ni/RM catalysts were prepared at different concentrations of nickel using wet impregnation method according to our previous studies.[44, 45] At room temperature the calculated amount of

$Ni(NO_3).6H_2O$ was dissolved in 100 ml deionized water and then mixed with RM (particle size<90 μm). The mixture was heated to 70 °C and continuously stirred for 5 hours to prepare the catalyst precursor. The catalyst precursor was dried at 105 °C for 10 hours and then calcined at 620 °C for 5 hours. The catalyst precursor was reduced for 6 hours at 450 °C using a reducing gas mixture of 10% H_2 and 90% N_2 at flow rate of 20 ml/min to obtain the tested catalyst, which was designated as x wt.% Ni/RM (x= 10, 20, 30, 40).

The catalysts were characterized by thermogravimetric-temperature programmed reduction (TG-TPR), Brunauer–Emmett–Teller (BET) surface area analyzer, X-ray diffraction (XRD), inductively coupling plasma (ICP) spectroscopy, and scanning electron microscopy (SEM) as reported previously.[44, 45]

2.5. Hydrodeoxygenation (HDO) experiments

HDO reactions were carried out in a Parr Series 4560 300 mL autoclave reactor (Parr Instruments, Moline, IL). The reactor can withstand a maximum pressure of 14 MPa at 500 ° C. A Parr 4848 controller was used to control the internal temperature and impeller speed. In a typical test, 100 g APPJCPO and catalyst (3 g) were loaded into the reactor. The reactor was flushed with hydrogen four times to purge the reactor vessel. High purity hydrogen was supplied from a reservoir tank via a pressure regulator. The reactor was then pressurized with hydrogen to 6.21 MPa (900 psi) at room temperature. A gas sample was taken from the gas sampling port for gas analysis when the reactor was at room temperature. The reactor was then heated to reaction temperature of 300, 350, or 400 °C. The reaction mixture was vigorously stirred (~1000 rpm) in order to eliminate diffusion limitations. The reaction time was recorded when the set temperature was reached. After the desired reaction time (30 minute), the reactor was cooled to room

temperature using the internal cooling coil and a gas sample was collected in a tedlar bag for analysis. The reproducibility of experiments was checked and the error in all experimental measurements was found to be less than 3%. Hydrogen consumption determination, product yields distribution, and gas analysis were carried out according to our previous work.[37] Conversion was calculated according to equation (1):

$$Conversion\ (\%) = \frac{(100-w_i).m_i-(100-w_f).m_f}{(100-w_{i)}.m_i} \times 100 \qquad (1)$$

Where w_i is the initial water content of APPJCPO (wt. %), m_i is the amount of APPJCPO loaded into the reactor (g), w_f is the water content of the aqueous phase after HDO (wt. %) and m_f is the amount of aqueous phase after HDO (g).

In blank experiments (without catalyst) 100 g of reaction mixture was charged into the reactor and the reactor was pressurized to 6.2 MPa (900 psi) with hydrogen and allowed to react for 30 minutes at 350 °C to determine if the reactor walls played any role in HDO reactions. All experiments were conducted in triplicate.

2.6. Analysis of HDO products

The liquid products of HDO experiments were analyzed for their elemental composition (CHNS-O), water content by Karl-Fischer titration, HHV, density, and viscosity. Details of these analysis are described elsewhere.[37]

The organic liquid products of HDO experiments (HDO oil) were analyzed by HPLC (Shimadzu Scientific, Columbia, MD, USA) using a RID-10A detector and a Kromasil 100-5-C18 column (AkzoNobel Amsterdam, Netherlands). The HPLC was equipped with a LC-10AT pump,

SCL-10Avp controller, and SIL-10A autosampler. CLASS-VP 7.3 SP1 software was used to analyze HPLC chromatograms. A CTO-10A column oven was used to maintain the column temperature at 55 °C during the analysis. The injection volume was 0.25 µl and acetonitrile at flow rate of 0.6 ml/min was used as the mobile phase. Data acquisition time was 80 minutes for all analyses. The identity of the HDO oil compounds were confirmed by GC/MS (Shimadzu GC/MS-QP5000, Shimadzu Scientific, Columbia, MD, USA).

The ^{13}C NMR spectra of the HDO oils were recorded on a BRUKER 500 MHz NMR spectrometer (Bruker Corporation, Japan). For sample preparation, about 0.3 g of the oil was dissolved in 0.9 g chloroform-d (Cambridge Isotope Laboratories, Inc., Tewksbury, MA, USA) in a 5-mm sample probe. The spectra were obtained with 3500 scans.

Thermal decomposition behavior of HDO oils were assessed by thermogravimetric analysis (TGA) using a TGA Q500 (TA Instruments, Lindon, UT, USA). Fifty milligrams of HDO oil was heated in high purity nitrogen flow from room temperature to 700 °C at a heating rate of 10 °C/min and the weight loss versus temperature was monitored. Weight loss curves were acquired by plotting the weight percent conversion versus temperature.

2.7. Catalyst deactivation

Previously we showed that three mechanisms contributed to the deactivation of Ni/RM catalyst; coke formation, oxidation, and formation of nickel iron oxide (Fe_2NiO_4).[44, 45] Herein we assessed the degree of oxidation by conducting TG-TPR of the used catalyst after HDO experiments. Details of TG-TPR analysis and coke formation evaluation is described elsewhere.[44, 45] Relative degree of oxidation (RDO) was calculated according to equation (2):

$$RDO = \frac{W_u}{W_c} \times 100 \qquad (2)$$

Where W_c is the amount of weight loss (wt. %) of fresh catalyst precursor (40%Ni/RM in calcined form) during reduction determined by TG-TPR (this value shows the maximum hydrogen uptake) and W_u is the weight loss (wt. %) of used catalyst due to reduction by TG-TPR (this value indicates the hydrogen uptake of used catalyst).

3. Results and discussion

The characterization of the red mud-supported nickel (Ni/RM) catalysts and the reduced red mud support (RRM) have been reported elsewhere[44, 45] and will not be repeated here. However, we repeat some important characteristics for clarity, thus the Brunauer-Emmette-Teller (BET) specific surface area of the calcined red mud was 37.5 m^2/g, that for the reduced red mud (RRM) was 54.3 m^2/g. Calcined NiO/RM at 10%, 20%, 30%, and 40% Ni loadings had BET specific surface areas of 40.2 m^2/g, 42.6 m^2/g, 46.7 m^2/g, and 51.3 m^2/g respectively. Reduced Ni/RM had specific surface areas of 65.5 m^2/g, 69.3 m^2/g, 73.4 m^2/g, and 79.3 m^2/g at 10%, 20%, 30%, and 40% Ni loadings respectively. The scanning electron microscopy (SEM) analysis of the surfaces of the catalysts were also published elsewhere,[44, 45] however, the Ni/RM surface showed a dispersion of Ni nano-particles of average size 90 nm. Because of this nano-particle dispersion, some areas of the surface were covered and there were gaps in between. This nano-particle dispersion was very important for the reactions described below because it allowed simultaneous reactions on the elemental Ni and the RRM. The BET specific siurface area of the commercial Ni/SiO_2-Al_2O_3 was 118.4 m^2/g.[44]

3.1. Characterization of APPJCPO

Table 1 shows the pH, water content, elemental composition, and chemical composition of APPJCPO. The presence of low molecular weight carboxylic acids in aqueous phase pyrolysis oil is the main reason for the acidic nature of APPJCPO (pH 2.97). The water content of APPJCPO was about 85 wt. % indicating presence of about 15% water soluble organic compounds. GC-MS analysis of APPJCPO organics were provided by Pacific Northwest National Laboratory (PNNL) (Table 1). The concentration of acetic acid in APPJCPO was 15.1 wt. % (water-free basis) which was the dominant compound in the APPJCPO. Other major compounds were acetone, furfural, 1-acetoxy-2-propanone, 1-hydroxy butanone, 1-hydroxy-2-propanone, guaiacol, 2,2-dimethyl-3-heptanone, 2,3-butanedione, and 3-hydroxy-2-butanone. As discussed in our previous works, RM catalyzed ketonization reactions,[46, 47] which could explain the dominance of ketones in the APPJCPO compared to pyrolysis using sand as the medium.[35]

Table 1: Characterization of APPJCPO.

Properties	value
pH	2.97
Water content (wt. %)	84.77
Elemental composition (wet basis)	
N	0.44
C	7.33
H	11.17
O	81.06
Chemical composition* (dry basis) (wt. %)	
Acetaldehyde	0.7
Acetic acid	15.1
Acetic anhydride	0.1
Acetone	2.4
Fructose	0.1
Furfural	6.8
Phenol	0.9
Xylose	0.3
1-acetoxy-2-propanone	2.3
1-hydroxy butanone	1.3
1-hydroxy-2-propanone	2.1
1,2-benzenediol	0.9
2-cyclopentene-1-one	0.6
2-methoxy phenol (guaiacol)	4.4
2-methyl phenol	0.2
2-methyl-1,4-benzenediol	0.3
2-methyl-2-cyclopentene-1-one	0.1
2,2-dimethyl-3-heptanone	1.2
2,3-butanedione	2.2
3-hydroxy-2-butanone	1.3
3-methyl-1,2-benzenediol	0.8
4-ethyl-1,3-benzenediol	0.4
4-methyl phenol	0.5
4-methyl-1,4-benzenediol	0.4

* Quantified ~ 45% of total carbon

3.2. HDO of APPJCPO using Ni/RM

3.2.1. Effect of Ni loading

The blank experiments showed no reactivity of the reactor walls. All results reported are therefore assumed to have no reactor wall influence. The results of HDO experiments using Ni/RM catalyst at different Ni loadings are shown in Table 2. RM in reduced form (RRM) was tested in HDO experiment to investigate the effect of catalyst support on the reactions. As shown in Table 2, the conversion of APPJCPO using RRM support was only 25.1% (Ni content of 0%) and the reaction produced 15.4% coke and 9.7% gas and a small amount of hydrogen (0.26 mol) was consumed. The liquid product consisted of one phase which had a pH of 6.11 compared to the raw feed that had a pH 2.97. The increased pH of the RRM HDO oil was attributed to ketonization of the carboxylic acids in the raw feed. The HPLC analysis of the liquid product showed reduced carboxylic acids content, especially acetic acid and increased concentrations of acetone and other ketones compared to the raw feed (see Tables 1 and 2). In addition to increased pH and ketone content and decrease in carboxylic acid concentration, the major gas produced was CO_2 which emanated from ketonization reactions.[48, 49] No hydrocarbons were detected in the liquid products. We previously showed that the presence of Ni is essential to partially reduce the oxygenated compounds of APPJCPO such as furfural and guaiacol to ethers.[46, 47] The ethers subsequently reacted with carbonyls on the RRM support to produce linear, branched, cyclic, aromatic, and alkylated aromatic hydrocarbons. In the absence of Ni, no ethers (furan, methyl furan, and anisole) were produced and hence no carbonyl alkylation reactions occurred. Ketonization, coke formation, as well as hydrocracking were the main reactions that occurred on the RRM (Table 2). The gaseous products were mostly CO and CO_2 (75 mole %) and the rest were C_1-C_5 hydrocarbons in very low concentrations.

When the APPJCPO was treated with 10 wt. % Ni/RM, the HDO liquid product consisted of one phase similar to the feed and its pH was 6.71. No detectable quantities of hydrocarbon liquid were produced but less coke was formed and gas yield doubled compared to 0%Ni HDO (Table 2). The liquid products had similar compounds as those found in the 0%Ni run and the raw feed.

The dominant gas component was methane, which was attributed to methanation of CO and CO_2 on the Ni sites, because the CO_2 content was relatively low compared to the 0%Ni and the water content was also higher (4.8%). The methane content of the gaseous product increased from 3.4 mole% in the 0%Ni to 58.2 mole% in the 10%Ni (Table 2), while ethane increased threefold, and propane increased very slightly. The increases in ethane and propane contents were attributed to hydrodeoxygenation of acetic acid, acetaldehyde, and acetone. In contrast, butane and pentane contents decreased relative to the 0%Ni HDO probably because of the cracking of these gases on the Ni sites. It can be surmised that the dominant reactions on the 10%Ni/RM were ketonization, methanation, hydrocracking and hydrodeoxygenation. In addition to ketonization reactions on the support material, gasification of some of the acetic acid could contribute to the slight increase in pH from 6.11 at 0% Ni to 6.71 at Ni loading of 10% (Table 2).

The reactions on the 20%, 30%, and 40% Ni loadings showed very interesting results because unlike the 0% and 10% Ni, the liquid products formed two immiscible phases comprising water and hydrocarbons and the pH ranged from 6.83 to 6.98 (Table 2). The liquid product (HDO oil) yields on Ni loadings of 20%, 30%, and 40% were 54.7%, 47.8%, and 23.9% respectively with oxygen contents of 3.45 wt. %, 1.14 wt. %, and 0.17 wt. % respectively. Although the 20%Ni had the highest hydrocarbon yield, it also had the highest oxygen content and furthermore, its aqueous phase contained unreacted material. In contrast, the 30% and 40% Ni HDO aqueous phase products

did not contain any detectable organic compounds and their pHs were neutral. Karl Fischer titration of these aqueous fractions showed about 99.5% water.

The HPLC and GC/MS analysis of the HDO organic liquid fraction showed a wide range of hydrocarbon compounds (Table 2). The formation of these liquid hydrocarbon compounds was attributed to "carbonyl alkylation" and hydrogenation reactions. The carbonyl alkylation reaction was due to the reaction of carbonyl compounds with unsaturated ethers such as anisole, furan, and methyl furan catalyzed by the reduced red mud (RRM) catalyst support. The aldehydes reacted with both furan and anisole but did not react with methylfuran, while the ketones reacted with methylfuran and anisole and not with furan. These complex reactions were catalyzed by the RRM and Ni through two pathways. First, when the concentration of the Ni on the RRM was about 20% or more, some fractions of acetic acid and other acids were reduced to aldehydes, furfural was reduced to furan and methyl furan, while guaiacol was reduced to anisole by the Ni. The RRM also catalyzed ketonization of some fraction of the acids to produce various ketones. The aldehydes and ketones then reacted with furan, methyl furan, and anisole catalyzed by the RRM to produce various hydrocarbons. The chain length of each hydrocarbon followed very simple rules: aldehydes reacting with furan form $C_{(n+4)}$ chain length where n is the number carbon atoms in the aldehyde compound; for ketones reacting with methyl furan the carbon chain length is $C_{(n+5)}$; for anisole reactions, both aldehydes and ketones follow the same rule, $C_{(n+6)}$ where n is the number of carbons in the carbonyl compounds. These carbonyl alkylation reactions produced alkylated benzenes and long chain aliphatic compounds such as ethyl benzene, isopropyl benzene, n-hexane, 2-methylheptane etc. (Table 2). In Table 2, there are another group of hydrocarbon compounds such as cyclopentane, cyclohexane, benzene, ethylcylohexane etc., which derived from hydrogenation of the carbonyl alkylation compounds and direct hydrodeoxygenation of guaiacol

that were attributed to catalysis by Ni. The Ni content appears to have direct influence on the formation of these compounds and their concentrations. The 20% Ni loading is at the threshold where there is enough Ni to catalyze the carbonyl alkylation, hydrodeoxygenation, and hydrogenation reactions. Above 20% Ni, the reaction was improved but there was a penalty due to hydrocracking of hydrocarbon compounds by Ni. The Ni loading on the red mud is important because it appeared that the ketonization of the carboxylic acids was very rapid and generated large amounts of CO_2, which then underwent methanation reaction on the Ni forming H_2O, CH_4 and coke. The coke rapidly fouled and deactivated the Ni and hence the partial reduction of furfural and guaiacol did not occur. Thus, when the Ni loading was 10% or less, there were not enough active sites to produce the ethers responsible for the carbonyl alkylation reactions. However, when the Ni loading was 20% or more, there was enough active sites to catalyze the ether production. When the Ni loading was above 30%, there were excess sites that catalyzed hydrocracking, hydrogenation, and hydrodeoxygenation reactions.

The APPJCPO conversion on Ni loadings of 30% and 40% were similar (99.5%) but there was a considerable difference in the deoxygenation of the HDO oil. The oxygen content of 30% Ni HDO oil was 1.14 wt. % compared to 0.17 wt. % for the 40% Ni HDO oil (Table 2). The increase in Ni loading from 30% to 40% increased the hydrocracking of the organic compounds, which subsequently resulted in increased gas yield from 41.6% to 65.85%.

The coke yields at various Ni loadings decreased with increasing Ni loadings. The support produced the highest coke (15.4%), but as the Ni loading increased this decreased from 15.4% to 1.7% at 40% Ni loading. The coke formation reactions appeared to be influenced by two factors, the Ni content of the catalysts and the water content of the reactants. The interaction of the Ni with the support appeared to lower the char formation because when the Ni content was increased there

was less exposed support material for the coke formation. The lower coke formation from HDO of APPJCPO was also attributed to the presence of about 85% water in the reaction mixture (APPJCPO), because water can moderate the coke formation.[46, 47] Furthermore, the chemical compounds of APPJCPO probably produced less coke compared to complicated components of ESP oil.

Table 2: Effect of Ni loading on the HDO of APPJCPO using Ni/RM catalyst (the reaction temperature was 350 °C).

Parameter	Ni loading (wt. %)				
	0	10	20	30	40
H_2 consumption (mol H_2)	0.26	1.16	1.35	1.63	1.87
Conversion (%)	25.1	31.8	93.3	99.5	99.5
Products yield distribution (based on initial organic content) (wt. %)					
HDO oil	0.0	0.0	54.7	47.8	23.9
Water*	0.0	4.8	6.5	7.1	7.8
Gas	9.7	18.5	27.4	41.6	65.8
Coke	15.4	8.5	4.7	2.4	1.7
Aqueous phase HDO product properties					
Water content (wt. %)	86.25	87.65	93.35	99.95	99.95
pH	6.11	6.71	6.83	6.97	6.98
HPLC analysis of aqueous phase HDO product (dry basis) (relative concentration wt. %)					
Acetaldehyde	0.6	0.2	0	0.0	0.0
Acetic acid	0.8	0.5	0.3	0.0	0.0
Acetone	14.3	12.7	3.4	0.0	0.0
Furfural	6.8	6.6	2.4	0.0	0.0
Phenol	1.1	1	0.5	0.0	0.0
1-hydroxy-2-propanone	2.6	2.2	1.3	0.0	0.0
2-cyclopentene-1-one	1.1	1.1	0.8	0.0	0.0
2-methoxy phenol (guaiacol)	4.3	4.3	1.8	0.0	0.0
2,2-dimethyl-3-heptanone	1.4	1.1	0.3	0.0	0.0
2,3-butanedione	3.5	2.5	1.1	0.0	0.0
3-hydroxy-2-butanone	1.6	1.4	0.6	0.0	0.0
Quantified % of organics	38.1	33.6	12.5	0.0	0.0
HDO oil properties					
HPLC analysis of HDO oil (relative concentration wt. %)					
Acetone	NA	NA	8.1	3.2	0.0
Benzene	NA	NA	7.4	2.2	1.8
Butanone	NA	NA	6.4	0.4	0.0
Cyclohexane	NA	NA	1.5	2.4	3.9
Cyclopentane	NA	NA	0.0	1.9	2.2
Ethylbenzene	NA	NA	7.2	17.8	2.7
Ethylcyclohexane	NA	NA	2.5	5.3	15.5
Isopropylbenzene	NA	NA	6.8	12.7	2.9
Isopropyl cyclohexane	NA	NA	2.3	4.7	13.8
Methanol	NA	NA	1.4	3.6	1.2
n-hexane	NA	NA	0.6	3.9	5.5
n-heptane	NA	NA	0.2	1.1	2.7
n-octane	NA	NA	0.3	0.9	2.9
Sec-butylbenzene	NA	NA	0.0	10.3	2.1
Toluene	NA	NA	1.4	3.8	5.1
Tetrahydrofuran	NA	NA	4.8	1.3	0.0
Xylene	NA	NA	1.3	4.1	1.9
2-methyloctane	NA	NA	3.2	4.5	6.2
2-methyltetrahydrofuran	NA	NA	3.5	0.8	0.0
2-pentanone	NA	NA	10.7	1.1	0.0
3-methylnonane	NA	NA	5.3	7.6	12.8
Quantified % of organics	NA	NA	74.9	93.6	83.2
Elemental composition of HDO oil (wt. %)					
N	NA**	NA	0.32	0.26	0.23
C	NA	NA	80.86	81.98	82.22
H	NA	NA	15.37	16.62	17.38
O	NA	NA	3.45	1.14	0.17
HHV (MJ/kg)	NA	NA	40.15	42.12	45.62
Density (g/ml)	NA	NA	0.89	0.82	0.77
Dynamic viscosity (cP)	NA	NA	2.54	1.46	1.22
Gas composition (mol %)					
CO	8.5	5.5	4.2	3.6	2.5
CO_2	66.6	12.1	10.3	8.4	6.3
CH_4	3.4	58.2	63.8	65.4	71.3
C_2H_6	2.2	6.3	6.9	7.1	7.3
C_3H_8	7.4	8.3	7.6	6.8	6.6
C_4H_{10}	6.1	5.4	4.3	4.2	4.1
C_5H_{12}	4.2	2.3	2.8	2.6	1.6

* By difference

** Not Applicable (no HDO oil produced)

3.2.2. Effect of reaction temperature

The 30%Ni/RM catalyst was used to investigate the effect of reaction temperature on the HDO products because this catalyst produced about 48% HDO oil with relatively low oxygen content compared to 20%Ni/RM and caused significantly less gasification than 40%Ni/RM (Table 2). The physico-chemical properties of HDO oils, product yields distribution, and gas analysis results after HDO of APPJCPO at reaction temperatures of 300, 350, and 400 °C are shown in Table 3. Increasing the reaction temperature improved HDO reactions but it also increased hydrocracking. The organic liquid yield after HDO at reaction temperatures of 300, 350, and 400 °C were 51.4 %, 47.8%, and 38.7% respectively with oxygen contents of 5.35 wt. %, 1.14 wt. % and 0.11 wt. % respectively. Increasing the reaction temperature negatively affected coke formation. The coke yield increased from 1.9% at 300 °C to 4.3% at 400 °C (Table 3).

When the HDO reaction temperature was increased from 300 °C to 400 °C the HHV of HDO oils increased from 38.77 MJ/kg to 45.71 MJ/kg because of improved hydrodeoxygenation and formation of more hydrocarbons through the carbonyl alkylation reactions. The major gas product was methane for all reaction temperatures because of methanation of CO and CO_2. The gas analysis showed that C_3 to C_5 hydrocarbon gases possibly underwent further hydrocracking at higher temperatures to produce methane and ethane because the molar concentration of these gases decreased with increase in reaction temperature (Table 3).

Table 3: Effect of reaction temperature on the HDO of APPJCPO using 30%Ni/RM catalyst.

Parameter	Reaction temperature (°C)		
	300	350	400
H_2 consumption (mol H_2)	1.24	1.63	1.96
Conversion (%)	88.1	99.5	99.6
Products yield distribution (based on initial organic content) (wt. %)			
HDO oil	51.4	47.8	38.7
Water*	3.3	7.1	8.3
Gas	31.5	41.6	48.3
Coke	1.9	2.4	4.3
Aqueous phase HDO product properties			
Water content (wt. %)	88.15	99.95	99.95
pH	6.02	6.97	6.98
HDO oil properties			
Elemental composition of HDO oil (wt. %)			
N	0.29	0.26	0.20
C	79.87	81.98	83.23
H	14.49	16.62	17.46
O	5.35	1.14	0.11
HHV (MJ/kg)	38.77	42.12	45.71
Density (g/ml)	0.91	0.82	0.75
Dynamic viscosity (cP)	3.67	1.46	1.20
Gas composition (mol %)			
CO	4.8	3.6	2.1
CO_2	10.2	8.4	5.5
CH_4	62.2	66.4	73.6
C_2H_6	5.8	7.1	8.3
C_3H_8	7.2	6.8	4.7
C_4H_{10}	5.4	4.2	3.1
C_5H_{12}	3.7	2.6	2.1

* By difference.

3.2.3. NMR of HDO oils

The ^{13}C NMR spectra of HDO at different reaction temperatures are shown in Figure 1. It can be clearly seen that increasing the reaction temperature influenced the chemical composition of the HDO oil. For better understanding of the process, semi-quantification of the NMR spectra shown in Figure 1 was carried out by integration of different chemical shift ranges.[37, 45, 50, 51] The semi-quantification of these spectra is presented in Table 4. At reaction temperature of 300 °C, carboxylic acids, aldehydes, and ketones were detected, but when the reaction temperature was increased to 400 °C, these signals disappeared. Increasing the reaction temperature also increased the amount of saturated aliphatic carbons due to saturation of double bonds and aromatic rings; consequently the amount of unsaturated aliphatic carbons and aromatic carbons decreased with increase in the reaction temperature.

The HDO oil at 350 °C had estimated research octane number (RON) of 77 and its ^{13}C NMR spectrum was similar to that of commercial gasoline[37] with the exception of a small fraction of aldehydes and ketones (1.2%, Table 4). The NMR results showed that at 350 °C, alcohols and methoxy phenols were converted to HDO products and carbonyl alkylation products respectively. At reaction temperature of 400 °C, the HDO oil contained only hydrocarbons and no oxygenated compounds were detected according to NMR spectra (Figure 1 and Table 4), thus, the 0.11% oxygen that was determined by elemental analysis (Table 3) was probably due to instrumental errors because the oxygen content was calculated by difference.

Table 4: Functional group distribution of HDO oils from ^{13}C NMR spectral integration at different reaction temperatures.

Chemical shift region (ppm)	Dominant type of carbon	Percentage of carbon based on ^{13}C NMR analysis		
		HDO oil- 300 °C	HDO oil- 350 °C	HDO oil- 400 °C
0-28	saturated aliphatic groups	35.3	39.3	54.6
28-55	unsaturated aliphatic groups	27.5	18.3	12.4
55-95	alcohols, ethers, phenolic methoxys, anhydrosugars	11.5	0.0	0.0
95-165	aromatics, furans	10.8	41.2	33.0
165-180	carboxylic acids, esters	9.5	0.0	0.0
180-215	ketones, aldehydes	5.4	1.2	0.0

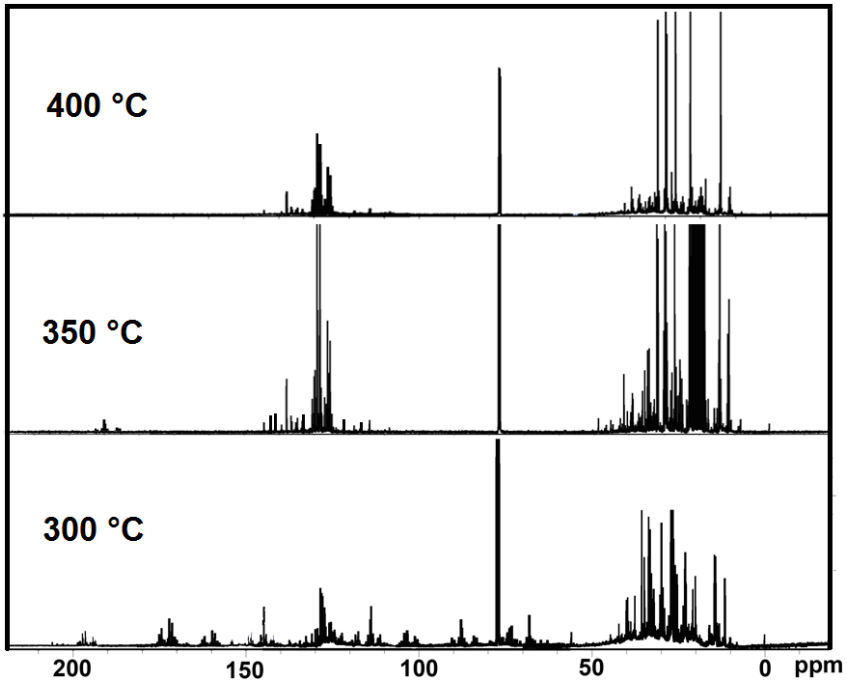

Figure 1: ^{13}C NMR spectra of APPJCPO HDO oils at different reaction temperatures.

3.2.4. Thermogravimetric analysis and chemical compounds of HDO oils

Figure 2 shows the weight loss behavior of HDO oils during thermogravimetric analysis under nitrogen atmosphere. The weight loss temperature ranges were classified as gasoline (30-180 °C), jet fuel (180-250 °C), diesel (250-350 °C), and heavy fuel (above 350 °C).[50] The HDO oil produced at reaction temperature of 300 °C had 67% gasoline range, 23% jet fuel range, and 10% diesel range hydrocarbons. The HDO oil at 350 °C contained 75% gasoline range and 25% jet fuel range hydrocarbon with no diesel range compounds. At reaction temperature of 400 °C the HDO oil was in gasoline range hydrocarbons with no jet fuel and diesel fraction (Figure 2). No heavy fuel range hydrocarbons were produced after HDO of APPJCPO at these reaction temperatures.

The HDO oil obtained at 350 °C using 30% Ni/RM was further analyzed by HPLC and GC-MS. The chemical compounds were classified into five major groups; aromatics, cyclic paraffins, internal olefins, linear paraffins, and oxygenates. These results are shown in Table 5. From these results it is clear that nearly all of the oxygenated compounds were converted to hydrocarbons by our method.

The carbon balance on the HDO products showed that the organic (liquid), aqueous, gas and coke phases contained 59.4 wt. %, 1.5 wt. %, 35.2 wt. %, and 3.8 wt.% respectively of the carbon in the original APPJCPO. The low carbon content for the aqueous phase indicated a very high concentration of oxygenates and low concentration of hydrocarbons. In addition, the pH of the aqueous phase was neutral at 6.9 indicating absence of acids.

Table 5: Classification of chemical compounds of APPJCPO HDO oil obtained at 350 °C using 30%Ni/RM.

Aromatics	Cyclic paraffins	Internal olefins	Linear paraffins	Oxygenates
Benzene	Cyclopentane	3-ethyl-non-6-ene	n-hexane	Acetone
Toluene	Cyclohexane	7-ethyl-undec-3-ene	n-heptane	2-methyltetrahydrofuran
Xylene	Ethylcyclohexane	7-isobutyl-undec-3-ene	n-octane	Tetrahydrofuran
Ethylbenzene	Isopropyl cyclohexane		2-methylheptane	Butanone
Isopropylbenzene			2-methyloctane	2-pentanone
Sec-butylbenzene			3-methyloctane	
			3-ethyloctane	
			3-methylnonane	
			3-ethylnonane	
			4-methylnonane	
			5-ethylundecane	
			5-isobutylundecane	

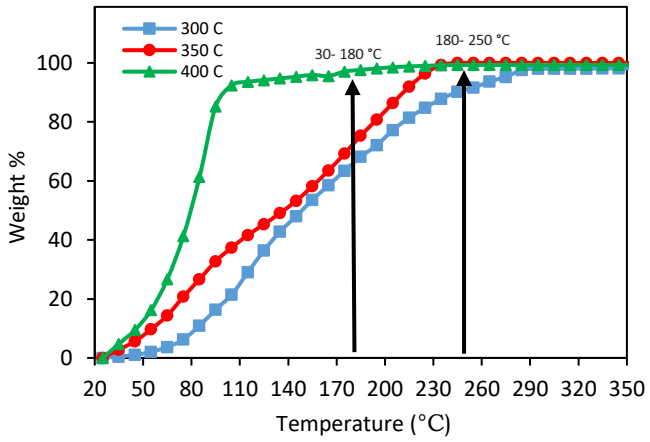

Figure 2: Petroleum equivalents of gasoline (30-180 °C), jet fuel (180-250 °C), and diesel (250- 350 °C) range hydrocarbons based on decomposition temperature weight present in APPJCPO HDO oils at different reaction temperatures.

3.3. HDO of APPJCPO using commercial Ni/SiO_2-Al_2O_3

For comparison, commercial Ni/SiO_2-Al_2O_3 (as received) which contained 63 wt.% Ni was used in HDO of APPJCPO under similar reaction conditions as the Ni/RM.[44] The APPJCPO conversions for this catalyst were 56.2%, 94.9% and 100% at reaction temperatures of 300 °C, 350 °C, and 400 °C respectively (Table 6). The liquid product was single phase that contained no hydrocarbon compounds, but were mostly oxygenates similar to the raw feed. The gas yield was significantly higher than that of Ni/RM catalyst (Table 6). Hydrogen consumption was more than

twice that of Ni/RM at all reaction temperatures. The higher activity of the commercial catalyst was attributed to higher amount of Ni loading and higher BET specific surface area.[44, 45] Unlike the RM support, the silica-alumina support did not catalyze carbonyl alkylation reactions. This catalyst deactivated more rapidly than Ni/RM when exposed to acids since it produced nearly three times more coke than Ni/RM at 350 °C. The pH of aqueous phase product at reaction temperatures of 300, 350, and 400 °C were 3.86, 5.19, and 6.97 (Table 6) respectively while the corresponding values for Ni/RM were 6.12, 6.97, and 6.98 respectively (Table 3). The commercial catalyst was less effective for the conversion of carboxylic acids because it did not catalyze ketonization reactions and only catalyzed hydrodeoxygenation reactions.

HPLC analysis of the Ni/SiO_2-Al_2O_3 aqueous phase products showed that at 300 °C, the concentration of acetic acid decreased from 15.1% to 7.8%, but the concentration of acetone did not change, which suggested that acetic acid was not ketonized to acetone. In contrast to Ni/RM, acetaldehyde concentration increased from 0.7% to 6.5 % because of the partial HDO of acetic acid. Thus, the increase in pH for the commercial catalyst was attributed to HDO of carboxylic acids on Ni metal and silica-alumina did not catalyze ketonization reactions. At higher reaction temperatures (350 and 400 °C), the oxygenated compounds of APPJCPO were gasified on the commercial catalyst (Table 6). For better comparison, we also investigated the HDO of APPJCPO using 65%Ni/RM (detailed data not provided). Although the liquid hydrocarbon yield decreased to 17.5 % at 65% Ni loading (compared to 24% using 40%Ni/RM), the chemical composition was similar to that of 40%Ni/RM. This would further conform the significant effect of RM support in producing liquid hydrocarbons by catalyzing carbonyl alkylation. The decrease in liquid yield was attributed to subsequent hydrocracking of produced hydrocarbons at higher Ni loading. This result was in agreement with our previous study.[45]

Table 6: HDO results of APPJCPO using commercial Ni/SiO_2-Al_2O_3 at different reaction temperatures.

Parameter	Reaction temperature (°C)		
	300	350	400
H_2 consumption (mol H_2)	2.35	3.77	4.45
Conversion (%)	56.2	94.9	100
Products yield distribution (based on initial organic content) (wt. %)			
HDO oil	0.0	0.0	0.0
Water*	5.5	15.3	18.4
Gas	45.3	73.5	74.8
Coke	5.4	6.1	6.8
Aqueous phase HDO product properties			
Water content (wt. %)	90.75	95.35	99.95
pH	3.86	5.19	6.97
HPLC analysis of aqueous phase HDO product (dry basis) (relative concentration wt. %)			
Acetaldehyde	6.5	0.2	0.0
Acetic acid	7.8	2.2	0.0
Acetone	2.3	1.4	0.0
Furfural	6.1	2.3	0.0
Phenol	0.6	0.1	0.0
1-hydroxy-2-propanone	1.6	0.7	0.0
2-cyclopentene-1-one	0.4	0.0	0.0
2-methoxy phenol (guaiacol)	3.8	1.1	0.0
2,2-dimethyl-3-heptanone	0.7	0.0	0.0
2,3-butanedione	1.7	0.3	0.0
3-hydroxy-2-butanone	0.8	0.2	0.0
Quantified % of organics	32.3	8.5	0.0
Gas composition (mol %)			
CO	2.5	0.0	0.0
CO_2	6.0	0.0	0.0
CH_4	81.2	92.1	94.0
C_2H_6	4.2	4.1	3.3
C_3H_8	2.5	2.1	1.5
C_4H_{10}	2.4	1.2	0.6
C_5H_{12}	0.7	0.3	0.1

* By difference.

3.4. Catalyst deactivation and regenerability

In order to examine the deactivation of the catalyst, Ni/RM was consecutively used in HDO of APPJCPO without any catalyst regeneration between runs. These tests were performed using the 40% Ni/RM to be able to investigate the effect of feed material on catalyst deactivation and compare them with the HDO of guaiacol as bio-oil model compound,[44] and HDO of the actual bio-oil (ESP oil) using this catalyst.[45] Table 7 shows the results of HDO experiments after each run. During the fourth run, no hydrocarbon was produced suggesting that deactivation of Ni occurred and consequently no HDO intermediates were produced for the carbonyl alkylation reactions on the RRM support. During the fourth run, although no hydrocarbon phase was produced, the pH of the liquid product was 4.82 and the concentration of ketones were relatively high (Table 7) and

the CO_2 (ketonization product) content was also high showing that ketonization reactions took place to some extent and the support still had some catalytic activity. There appeared to be complete deactivation of both Ni and the support during the sixth run, because the pH of aqueous phase was 2.98 (Table 7). Furthermore, no CO_2 (product of ketonization) was produced during the sixth run and the reaction only produced coke (Table 7). Previously, we showed that the catalyst deactivation was due to oxidation of Ni, coke formation, and formation of nickel iron oxide (Fe_2NiO_4).[44, 45] Herein we focused on the effect of coke formation and oxidation on catalyst deactivation.

Because coke formation can reduce the BET specific surface area,[52, 53] the BET specific surface area (Table 7) was plotted against coke yield (Figure 3) for HDO of APPJCPO, guaiacol,[44] and ESP oil[45] to compare the effect of feedstock on catalyst deactivation. According to Figure 3, in the case of APPJCPO the data points fitted well to linear regression (R^2 of 0.99) but in the case of ESP oil and guaiacol the data points were more scattered (R^2 of 0.83 and 0.89 respectively). These results suggested that coke formation was possibly the major pathway for catalyst deactivation during HDO of APPJCPO, whereas oxidation could have a higher contribution to catalyst deactivation in the case of ESP oil and guaiacol.

Figure 4 shows the TG-TPR of fresh catalyst (40%Ni/RM in reduced form), catalyst precursor (40%Ni/RM in calcined form), completely deactivated catalyst after HDO of APPJCPO (after 6 runs), and completely deactivated catalyst after HDO of ESP oil[45] (after 4 runs). The fresh catalyst did not show any reduction peaks because the catalyst was in reduced form. The catalyst precursor showed two major reduction peaks at 442°C and 583°C. The peak at 442°C appeared to have higher concentration of NiO than the 583°C peak as described previously.[45] There were no distinct peaks for RM and NiO because of interaction between NiO and the support.[44, 45] The TG-

TPR profile of deactivated catalyst after HDO of ESP oil[45] showed three reduction peaks at 341°C, 477°C, and 640°C. The peak at 341°C was attributed to reduction of free NiO because its reduction temperature was close to that of NiO as reported previously.[44, 45] The other two peaks were due to the reduction of bulk phase NiO where there was interaction between NiO and RM support. The peak at 477°C was probably due to reduction of surface components of Ni/RM in the bulk phase and the peak at 640°C was possibly due to reduction of catalyst components inside the bulk phase because they had a higher reduction temperature due to mass transfer limitation to inside components. This result appeared to suggest that during HDO of ESP oil, some Ni particles lost their interactions with the support material and underwent oxidation, in addition to the oxidation of bulk phase Ni/RM.

The TG-TPR profile of deactivated catalyst after HDO of APPJCPO showed only one reduction peak at 325°C (Figure 4). This peak was attributed to reduction of free NiO. This result seemed to suggest that during the HDO of APPJCPO some Ni particles lost their interactions with RM support and underwent oxidation. In contrast to HDO of ESP oil, the oxidation of bulk phase NiO did not occur because the TPR profile did not show any reduction peak between 442°C and 700°C.[42] The aqueous phase (water) appeared to inhibit the oxidation of bulk phase NiO as compared to HDO of the ESP bio-oil.[42] The RDO after complete deactivation of catalyst was 27.8% for APPJCPO compared to 76.4% in the case of ESP oil. Hence, coke formation was probably the major pathway for catalyst deactivation during HDO of APPJCPO, while oxidation and coke formation were both significant factors in the deactivation of Ni/RM during HDO of ESP oil.

Table 7: Catalyst deactivation during HDO of APPJCPO using 40% Ni/RM (reaction temperature of 350 °C).

Parameter	Reuse #					
	Fresh	Reuse# 1	Reuse #2	Reuse #3	Reuse #4	Reuse #5
Catalyst BET specific surface area (m^2/g)	79.3	76.6	72.7	70.4	67.6	63.1
H_2 consumption (mol H_2)	1.87	1.51	1.19	0.96	0.15	0.00
Conversion (%)	99.5	75.7	68.1	25.7	16.0	9.7
Products yield distribution (based on initial organic content) (wt. %)						
HDO oil	23.9	33.5	40.5	0.0	0.0	0.0
Water*	7.8	5.7	4.1	3.5	0.0	0.0
Gas	65.8	34.2	19.4	16.7	8.2	0.0
Coke	1.7	2.3	4.1	5.5	7.8	9.7
Aqueous phase HDO product properties						
Water content (wt. %)	99.95	94.45	91.20	88.05	86.25	84.85
pH	6.98	6.84	6.37	4.82	3.75	2.98
HPLC analysis of aqueous phase HDO product (dry basis) (relative concentration wt. %)						
Acetaldehyde	0.0	0.0	0.0	0.2	0.5	0.7
Acetic acid	0.0	0.3	0.6	3.4	8.1	15.1
Acetone	0.0	3.9	7.3	6.6	5.5	2.4
Furfural	0.0	0.0	0.0	2.7	6.2	6.8
Phenol	0.0	0.0	0.0	0.6	0.7	0.9
1-hydroxy-2-propanone	0.0	1.1	3.5	3.2	2.6	2.1
2-cyclopentene-1-one	0.0	0.0	0.9	0.7	0.6	0.6
2-methoxy phenol (guaiacol)	0.0	0.0	0.0	1.6	3.9	4.4
2,2-dimethyl-3-heptanone	0.0	0.0	2.3	1.7	1.4	1.2
2,3-butanedione	0.0	0.0	3.4	2.7	2.5	2.2
3-hydroxy-2-butanone	0.0	0.0	0.0	1.9	1.6	1.3
Quantified % of organics	0.0	5.3	18.0	25.3	33.6	37.7
HDO oil properties						
HPLC analysis of HDO oil (relative concentration wt. %)						
Acetone	0.0	0.5	1.1	NA	NA	NA
Benzene	1.8	0.7	0.3	NA	NA	NA
Butanone	0.0	5.2	9.1	NA	NA	NA
Cyclohexane	3.9	1.5	0.0	NA	NA	NA
Cyclopentane	2.2	0.7	0.0	NA	NA	NA
Ethylbenzene	2.7	1.5	0.8	NA	NA	NA
Ethylcyclohexane	15.5	9.5	4.2	NA	NA	NA
Isopropylbenzene	2.9	1.6	0.7	NA	NA	NA
Isopropyl cyclohexane	13.8	6.3	3.4	NA	NA	NA
Methanol	1.2	1.0	0.5	NA	NA	NA
n-hexane	5.5	4.2	3.5	NA	NA	NA
n-heptane	2.7	1.5	1.1	NA	NA	NA
n-octane	2.9	1.2	0.6	NA	NA	NA
Sec-butylbenzene	2.1	1.0	0.3	NA	NA	NA
Toluene	5.1	4.1	2.1	NA	NA	NA
Tetrahydrofuran	0.0	1.1	2.8	NA	NA	NA
Xylene	1.9	0.7	0.0	NA	NA	NA
2-methyloctane	6.2	3.4	1.7	NA	NA	NA
2-methyltetrahydrofuran	0.0	0.7	3.1	NA	NA	NA
2-pentanone	0.0	4.1	10.3	NA	NA	NA
3-methylnonane	12.8	7.3	3.7	NA	NA	NA
Quantified % of organics	83.2	57.8	49.3	NA	NA	NA
Elemental composition of HDO oil (wt. %)						
N	0.23	0.27	0.30	NA**	NA	NA
C	82.22	81.03	77.56	NA	NA	NA
H	17.38	15.46	13.27	NA	NA	NA
O	0.17	3.24	8.87	NA	NA	NA
HHV (MJ/kg)	45.62	40.26	33.42	NA	NA	NA
Density (g/ml)	0.77	0.85	0.92	NA	NA	NA
Dynamic viscosity (cP)	1.22	2.36	4.16	NA	NA	NA
Gas composition (mol %)						
CO	2.5	3.6	10.1	19.6	36.0	0.0
CO_2	6.3	7.8	10.3	15.8	19.4	0.0
CH_4	71.3	63.2	54.8	37.3	13.1	0.0
C_2H_6	7.3	6.7	5.4	4.0	3.8	0.0
C_3H_8	6.6	8.5	9.0	11.6	13.6	0.0
C_4H_{10}	4.1	4.8	5.5	6.3	6.9	0.0
C_5H_{12}	1.6	3.7	4.3	5.2	6.2	0.0

* By difference

** Not Applicable (no HDO oil produced)

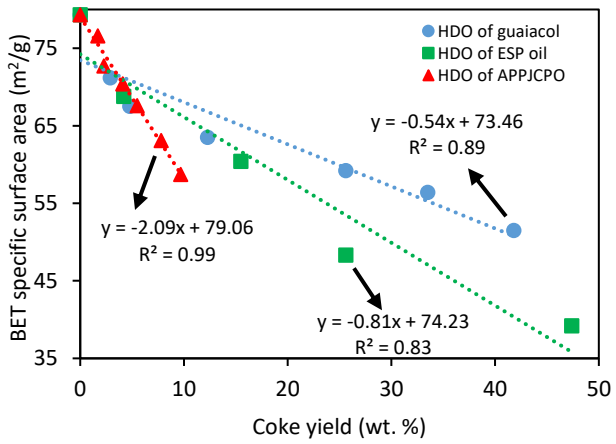

Figure 3: Catalyst BET specific surface area vs. coke yield during consecutive reuse of 40%Ni/RM without regeneration between runs for HDO of guaiacol[44] (reprinted in part with permission from Elsevier), ESP oil[45] (reprinted in part with permission from Elsevier), and APPJCPO.

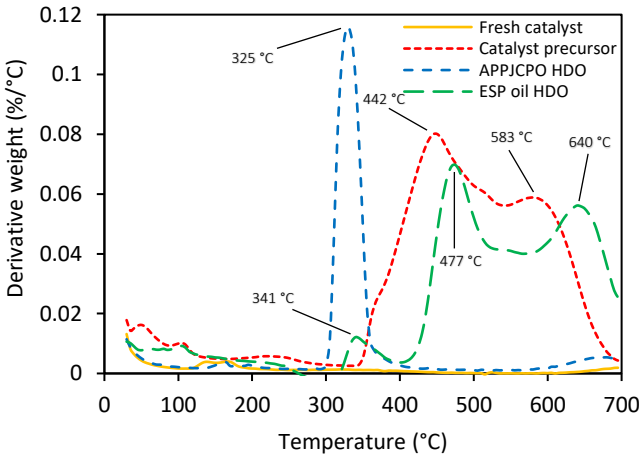

Figure 4: TG-TPR profiles of 40%Ni/RM; fresh catalyst (reduced form) (yellow), catalyst precursor (calcined form) (red), deactivated catalyst after HDO of APPJCPO (blue), and deactivated catalyst after HDO of ESP oil[45] (reprinted in part with permission from Elsevier) (green).

The TG-TPR profiles of used Ni/RM after each run is shown in Figure 5. It was clear that after each run more Ni particles lost their interactions with RM support and underwent oxidation because the intensity of NiO reduction peak (~325°C) increased after each HDO experiment. In

addition to coke formation, oxidation can contribute to the reduction in BET specific surface area.[54-56] The RDO of catalyst after each run showed the reduction in BET specific surface area (Figure 6). The linear regression of the BET specific surface area against RDO (Figure 6) showed more scatter compared to BET specific surface area versus coke yield (Figure 3) suggesting that after complete deactivation of the catalyst some Ni particles were still in the bulk phase and retained their interaction with RM support. After six runs, because no bulk phase reduction peaks were observed in the TPR profile of the catalyst, this could suggest that the deactivation of Ni was mostly due to oxidation and loss of interaction with RM support, whereas the deactivation of RM support was mainly because of coke formation.

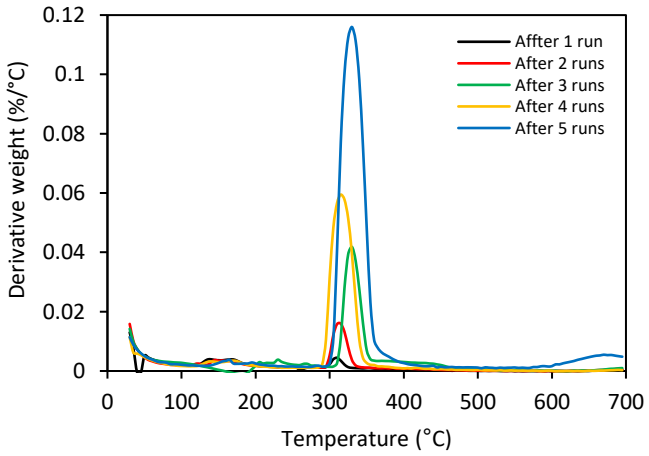

Figure 5: TG-TPR profiles of 40%Ni/RM after consecutive reuse of the catalyst without regeneration between runs after HDO of APPJCPO.

Overall, these results (Figures 3-6) suggested that two major mechanisms contributed to change in BET specific surface area; coke formation and oxidation. According to Jahromi and Agblevor[45] the BET specific surface area of RM in calcined and reduced forms were 37.5 and 54.3 m^2/g respectively, while the BET specific surface area of 40%Ni/RM in calcined and reduced form were 51.3 and 79.3 m^2/g respectively. Therefore, the reduction process increased the BET specific

surface area of RM and 40%Ni/RM by 44.8% and 54.5% respectively which shows that Ni redox state has a greater influence on BET specific surface area than RM redox state. During HDO of APPJCPO only oxidation of Ni took place, whereas during HDO of ESP oil and guaiacol, the RM underwent oxidation and Ni oxidation was much less pronounced (Figure 4). Thus, the change in BET specific surface area was more affected by coke formation in HDO of ESP oil and guaiacol, while this parameter was more influenced by oxidation of Ni after HDO of APPJCPO. Hence, although less coke was produced in the case of APPJCPO, a greater slope was observed for APPJCPO in Figure 3 due to more oxidation of Ni.

The deactivated Ni/RM catalyst (after 6 HDO runs) was regenerated by burning off the coke at 400°C in a muffle furnace followed by reduction at 450°C using a reducing gas mixture of 10% H_2 and 90% N_2 according to our previous studies.[44, 45] The catalyst activity was completely restored after regeneration (data not provided), however the regeneration of the commercial Ni/SiO_2-Al_2O_3 was not possible following the same procedure and the catalyst did not have HDO activity after reduction (data not provided). Additionally, when exposed to air, the reduced commercial catalyst caught fire due to spontaneous oxidation, whereas the reduced Ni/RM was stable on exposure to air.

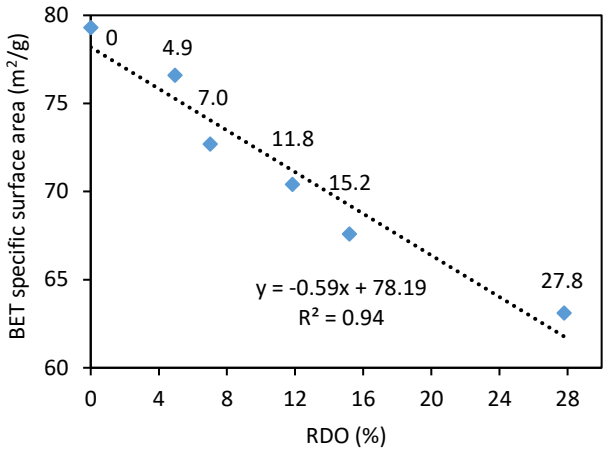

Figure 6: BET specific surface area versus RDO during consecutive HDO experiments without regeneration between runs (data labels show RDO % values).

4. Conclusion

Hydrodeoxygenation (HDO) of aqueous phase pinyon-juniper catalytic pyrolysis oil (APPJCPO) was studied using a new multifunctional Ni/RM catalyst at different Ni loadings and reaction temperatures. The HDO of APPJCPO produced liquid, gas, and solid products. The liquid product consisted of aqueous phase and organic phase (HDO oil). The HDO oil yield at reaction temperature of 350°C using 30%Ni/RM was 47.8% with oxygen content of 1.14 wt. % that consisted of 75% gasoline fraction and 25% jet fuel fraction based on boiling point temperature ranges. For comparison, commercial Ni/SiO_2-Al_2O_3 used in HDO experiments under similar conditions gasified the organic compounds of APPJCPO and did not produce any liquid hydrocarbon. The key for the production of HDO oil on Ni/RM was the cross-reactions of HDO intermediates on the support. In the case of Ni/RM, the oxygenated compounds in APPJCPO first underwent partial reduction on Ni sites. These reduction intermediates underwent carbonyl alkylation on the support material to produce aliphatics and alkylated aromatics. Whereas in the case of the commercial catalyst, silica-alumina did not catalyze the carbonyl alkylation reactions

so no liquid hydrocarbons were produced. Furthermore, RM catalyzed ketonization reactions that increased the pH of the aqueous phase to about neutral even in the absence of Ni. Coke formation and Ni oxidation appeared to be the major controlling factors for catalyst deactivation. TG-TPR results showed that some Ni particles lost their interaction with the RM support and underwent oxidation but oxidation of bulk phase Ni did not take place. Coke formation was the major cause of deactivation of the support material. This study showed that Ni/RM can serve as a multifunctional catalyst that can be used in the production of liquid hydrocarbons from low molecular weight oxygenates that are present in aqueous phase pyrolysis oils.

Acknowledgement

We wish to acknowledge funding support by the National Science Foundation under contract # 1445735 and Utah Science Technology and Research (USTAR) Program. We also thank Garret Smith, Kyle Christian, and Brandon Sargent for producing the APPJCPO. Dr Karl Albrecht, formerly of PNNL is acknowledged for analyzing the APPJCPO. A portion of this research was conducted as part of Co-Optimization of Fuels and Engines (Co-Optima) project funded by the U.S. Department of Energy Office of Energy Efficiency and Renewable Energy, Bioenergy Technologies and Vehicle Technologies Offices.

References

(1) Huber, G. W.; Iborra, S.; Corma, A. Synthesis of Transportation Fuels from Biomass: Chemistry, Catalysts, and Engineering. *Chem. Rev.* **2006**, *106* (9), 4044–4098.

(2) Lee, H.; Kim, Y.; Lee, I.; Jeon, J.; Jung, S.; Chung, J. Do; Choi, W. G.; Park, Y. Recent Advances in the Catalytic Hydrodeoxygenation of Bio-Oil. **2016**, *33* (12), 3299–3315.

(3) Xiu, S.; Shahbazi, A. Bio-Oil Production and Upgrading Research: A Review. *Renew. Sustain. Energy Rev.* **2012**, *16* (7), 4406–4414.

(4) Sanna, A.; Vispute, T. P.; Huber, G. W. Hydrodeoxygenation of the Aqueous Fraction of Bio-Oil with Ru/C and Pt/C Catalysts. *Appl. Catal. B Environ.* **2015**, *165*, 446–456.

(5) Abnisa, F.; Wan Daud, W. M. A.; Arami-Niya, A.; Ali, B. S.; Sahu, J. N. Recovery of Liquid Fuel from the Aqueous Phase of Pyrolysis Oil Using Catalytic Conversion. *Energy & Fuels* **2014**, *28* (5), 3074–3085.

(6) Jain, A. B.; Vaidya, P. D. Kinetics of Aqueous-Phase Hydrogenation of Model Bio-Oil Compounds over a Ru/C Catalyst. *Energy and Fuels* **2015**, *29* (1), 361–368.

(7) Vispute, T. P.; Huber, G. W. Production of Hydrogen, Alkanes and Polyols by Aqueous Phase Processing of Wood-Derived Pyrolysis Oils. *Green Chem.* **2009**, *11* (9), 1433.

(8) Li, N.; Tompsett, G. A.; Zhang, T.; Shi, J.; Wyman, C. E.; Huber, G. W. Renewable Gasoline from Aqueous Phase Hydrodeoxygenation of Aqueous Sugar Solutions Prepared by Hydrolysis of Maple Wood. *Green Chem.* **2011**, *13* (1), 91–101.

(9) Lee, Y.; Shafaghat, H.; Kim, J.; Jeon, J. K.; Jung, S. C.; Lee, I. G.; Park, Y. K. Upgrading of Pyrolysis Bio-Oil Using WO_3/ZrO_2 and Amberlyst Catalysts: Evaluation of Acid Number and Viscosity. *Korean J. Chem. Eng.* **2017**, *34* (8), 2180–2187.

(10) Kim, H.; Shafaghat, H.; Kim, J.; Kang, B. S.; Jeon, J. K.; Jung, S. C.; Lee, I. G.; Park, Y. K. Stabilization of Bio-Oil over a Low Cost Dolomite Catalyst. *Korean J. Chem. Eng.* **2018**, *35* (4), 922–925.

(11) Huber, G. W.; Chheda, J. N.; Barrett, Ch. J.; Dumesic, J. A. Production of Liquid Alkanes by Aqueous-Phase Processing of Biomass-Derived Carbohydrates. *Science* **2005**, *308*, 306–311.

(12) Zhang, X.; Wang, T.; Ma, L.; Zhang, Q.; Jiang, T. Hydrotreatment of Bio-Oil over Ni-Based Catalyst. *Bioresour. Technol.* **2013**, *127*, 306–311.

(13) Furimsky, E. Catalytic Hydrodeoxygenation. *Appl. Catal. A Gen.* **2000**, *199* (2), 147–190.

(14) Li, N.; Tompsett, G. A.; Huber, G. W. Renewable High-Octane Gasoline by Aqueous-Phase Hydrodeoxygenation of C5 and C6 Carbohydrates over Pt/zirconium Phosphate Catalysts. *ChemSusChem* **2010**, *3* (10), 1154–1157.

(15) Dongil, A. B.; Pastor-Pérez, L.; Sepúlveda-Escribano, A.; García, R.; Escalona, N. Hydrodeoxygenation of Guaiacol: Tuning the Selectivity to Cyclohexene by Introducing Ni Nanoparticles inside Carbon Nanotubes. *Fuel* **2016**, *172*, 65–69.

(16) Tran, N. T. T.; Uemura, Y.; Chowdhury, S.; Ramli, A. Vapor-Phase Hydrodeoxygenation of Guaiacol on Al-MCM-41 Supported Ni and Co Catalysts. *Appl. Catal. A Gen.* **2016**, *512*, 93–100.

(17) Mora-Vergara, I. D.; Hernández Moscoso, L.; Gaigneaux, E. M.; Giraldo, S. A.; Baldovino-Medrano, V. G. Hydrodeoxygenation of Guaiacol Using NiMo and CoMo Catalysts Supported on Alumina Modified with Potassium. *Catal. Today* **2018**, *302*, 125–135.

(18) Manikandan, M.; Venugopal, A. K.; Prabu, K.; Jha, R. K.; Thirumalaiswamy, R. Role of Surface Synergistic Effect on the Performance of Ni-Based Hydrotalcite Catalyst for Highly Efficient Hydrogenation of Furfural. *J. Mol. Catal. A Chem.* **2016**, *417*, 153–162.

(19) Xiong, K.; Wan, W.; Chen, J. G. Reaction Pathways of Furfural, Furfuryl Alcohol and 2-Methylfuran on Cu(111) and NiCu Bimetallic Surfaces. *Surf. Sci.* **2016**, *652*, 91–97.

(20) Zhang, C.; Lai, Q.; Holles, J. H. Bimetallic Overlayer Catalysts with High Selectivity and Reactivity for Furfural Hydrogenation. *Catal. Commun.* **2017**, *89*, 77–80.

(21) Wang, C.; Luo, J.; Liao, V.; Lee, J. D.; Onn, T. M.; Murray, C. B.; Gorte, R. J. A Comparison of Furfural Hydrodeoxygenation over Pt-Co and Ni-Fe Catalysts at High and Low H2pressures. *Catal. Today* **2018**, *302*, 73–79.

(22) Fu, Z.; Wang, Z.; Lin, W.; Song, W.; Li, S. High Efficient Conversion of Furfural to 2-Methylfuran over Ni-Cu/Al2O3catalyst with Formic Acid as a Hydrogen Donor. *Appl. Catal. A Gen.* **2017**, *547* (August), 248–255.

(23) He, Z.; Wang, X. Required Catalytic Properties for Alkane Production from Carboxylic Acids: Hydrodeoxygenation of Acetic Acid. *J. Energy Chem.* **2013**, *22* (6), 883–894.

(24) Onyestyák, G.; Harnos, S.; Klébert, S.; Štolcová, M.; Kaszonyi, A.; Kalló, D. Selective Reduction of Acetic Acid to Ethanol over Novel Cu2In/Al2O3catalyst. *Appl. Catal. A Gen.* **2013**, *464–465*, 313–321.

(25) Badari, A. C.; Harnos, S.; Lónyi, F.; Onyestyák, G.; Štolcová, M.; Kaszonyi, A.; Valyon, J. A Study of the Selective Catalytic Hydroconversion of Biomass-Derived Pyrolysis or Fermentation Liquids Using Propylamine and Acetic Acid as Model Reactants. *Catal. Commun.* **2014**, *58*, 1–5.

(26) Elliott, D. C.; Hart, T. R. 73 Catalytic Hydroprocessing of Chemical Models for Bio-Oil. *Energy and Fuels* **2009**, 8, 631–637.

(27) Wang, J.; Luo, Z.; Zhang, J.; Dang, Q.; Chen, W. Reactions of Furfural and Acetic Acid as Model Compounds for Bio-Oil Upgrading in Supercritical Ethanol. *Int. Conf. Electron. Commun. Control. ICECC* **2011**, *2*, 1587–1592.

(28) Si, Z.; Zhang, X.; Wang, C.; Ma, L.; Dong, R. An Overview on Catalytic Hydrodeoxygenation of Pyrolysis Oil and Its Model Compounds. *Catalysts* **2017**, *7* (6), 169.

(29) Power, G.; Gräfe, M.; Klauber, C. Bauxite Residue Issues: I. Current Management, Disposal and Storage Practices. *Hydrometallurgy* **2011**, *108* , 33–45.

(30) Wang, S.; Ang, H. M.; Tadé, M. O. Novel Applications of Red Mud as Coagulant, Adsorbent and Catalyst for Environmentally Benign Processes. *Chemosphere* **2008**, *72* (11), 1621–1635.

(31) Sushil, S.; Batra, V. S. Catalytic Applications of Red Mud , an Aluminium Industry Waste : A Review. *Appl. Catal. B Envison.* **2008**, *81*, 64–77.

(32) Hua, Y.; Heal, K. V.; Friesl-Hanl, W. The Use of Red Mud as an Immobiliser for Metal/metalloid-Contaminated Soil: A Review. *J. Hazard. Mater.* **2017**, *325*, 17–30.

(33) Liu, Y.; Naidu, R. Hidden Values in Bauxite Residue (Red Mud): Recovery of Metals. *Waste Manag.* **2014**, *34*, 2662–2673.

(34) Liu, X.; Zhang, N. Utilization of Red Mud in Cement Production: A Review. *Waste Manag. Res.* **2011**, *29*, 1053–1063.

(35) Yathavan, B. K.; Agblevor, F. A. Catalytic Pyrolysis of Pinyon-Juniper Using Red Mud and HZSM-5. *Energy and Fuels* **2013**, *27*, 6858–6865.

(36) Xu, B.; Qi, F.; Zhang, J.; Li, H.; Sun, D.; Robert, D.; Chen, Z. Cobalt Modified Red Mud Catalytic Ozonation for the Degradation of Bezafibrate in Water: Catalyst Surface Properties Characterization and Reaction Mechanism. *Chem. Eng. J.* **2016**, *284*, 942–952.

(37) Jahromi, H.; Agblevor, F. A. Upgrading of Pinyon-Juniper Catalytic Pyrolysis Oil via Hydrodeoxygenation. *Energy* **2017**, *141*, 2186–2195.

(38) Shim, W. G.; Nah, J. W.; Jung, H. Y.; Park, Y. K.; Jung, S. C.; Kim, S. C. Recycling of Red Mud as a Catalyst for Complete Oxidation of Benzene. *J. Ind. Eng. Chem.* **2018**, *60*, 259–267.

(39) Santona, L.; Castaldi, P.; Melis, P. Evaluation of the Interaction Mechanisms between Red Muds and Heavy Metals. *J. Hazard. Mater.* **2006**, *136*, 324–329.

(40) Pappu, A.; Saxena, M.; Asolekar, S. R. Solid Wastes Generation in India and Their Recycling Potential in Building Materials. *Build. Environ.* **2007**, *42* (6), 2311–2320.

(41) Li, Y.; Liu, C.; Luan, Z.; Peng, X.; Zhu, C.; Chen, Z.; Zhang, Z.; Fan, J.; Jia, Z. Phosphate Removal from Aqueous Solutions Using Raw and Activated Red Mud and Fly Ash. *J. Hazard. Mater.* **2006**, *137*, 374–383.

(42) Liu, Z.; Li, H. Metallurgical Process for Valuable Elements Recovery from Red Mud - A Review. *Hydrometallurgy* **2015**, *155*, 29–43.

(43) Mante, O. D.; Agblevor F. A. Catalytic Pyrolysis for the Production of Refinery-Ready Biocrude oils from Six Different Biomass Sources. *Green Chem.* **2014**, 16, 3364-3377.

(44) Jahromi, H.; Agblevor, F. A. Hydrotreating of Guaiacol: A Comparative Study of Red Mud-Supported Nickel and Commercial Ni/SiO_2-Al_2O_3catalysts. *Appl. Catal. A Gen.* **2018**, *558*, 109–121.

(45) Jahromi, H.; Agblevor, F. A. Hydrodeoxygenation of Pinyon-Juniper Catalytic Pyrolysis Oil Using Red Mud-Supported Nickel Catalysts. *Applied Catal. B, Environ.* **2018**, *236* (2010), 1–12.

(46) Agblevor, F. A.; Jahromi, H. Aqueous Phase Synthesis of Hydrocarbons from Furfural Reactions with Low Molecular Weight Biomass Oxygenates. *Energy and Fuels* **2018**, *32*, 8552–8562.

(47) Agblevor, F. A.; Jahromi, H. Aqueous Phase Synthesis of Hydrocarbons from Reactions of Guaiacol and Low Molecular Weight Oxygenates. *ChemCatChem* **2018**, accepted article. https://doi.org/10.1002/cctc.201800982.

(48) Joshi, N.; Lawal, A. Hydrodeoxygenation of Acetic Acid in a Microreactor. *Chem. Eng. Sci.* **2012**, *84*, 761–771.

(49) Baylon, R. A. L.; Sun, J.; Martin, K. J.; Venkitasubramanian, P.; Wang, Y. Beyond Ketonization: Selective Conversion of Carboxylic Acids to Olefins over Balanced Lewis Acid–base Pairs. *Chem. Commun.* **2016**, *52*, 4975–4978.

(50) Zhang, X.; Chen, L.; Kong, W.; Wang, T.; Zhang, Q.; Long, J.; Xu, Y.; Ma, L. Upgrading of Bio-Oil to Boiler Fuel by Catalytic Hydrotreatment and Esterification in an Efficient Process. **2015**, *84*, 83–90.

(51) Tanneru, S. K.; Steele, P. H. Pretreating Bio-Oil to Increase Yield and Reduce Char during Hydrodeoxygenation to Produce Hydrocarbons. *Fuel* **2014**, *133*, 326–331.

(52) Li, Y.; Zhang, C.; Liu, Y.; Tang, S.; Chen, G.; Zhang, R.; Tang, X. Coke Formation on the Surface of Ni/HZSM-5 and Ni-Cu/HZSM-5 Catalysts during Bio-Oil Hydrodeoxygenation. *Fuel* **2017**, *189*, 23–31.

(53) Wan, Z.; Li, G. K.; Wang, C.; Yang, H.; Zhang, D. Relating Coke Formation and Characteristics to Deactivation of ZSM-5 Zeolite in Methanol to Gasoline Conversion. *Appl. Catal. A Gen.* **2018**, *549*, 141–151.

(54) Chenna, S.; Banerjee, R.; Crozier, P. A. Atomic-Scale Observation of the Ni Activation Process for Partial Oxidation of Methane Using In Situ Environmental TEM. *Chem. Cat. Chem.* **2011**, *3*, 1051–1059.

(55) Jeangros, Q.; Hansen, T. W.; Wagner, J. B.; Damsgaard, C. D.; Dunin-Borkowski, R. E.; Hébert, C.; Van Herle, J.; Hessler-Wyser, A. Reduction of Nickel Oxide Particles by Hydrogen Studied in an Environmental TEM. *J. Mater. Sci.* **2013**, *48*, 2893–2907.

(56) Coronado, I.; Stekrova, M.; García Moreno, L.; Reinikainen, M.; Simell, P.; Karinen, R.; Lehtonen, J. Aqueous-Phase Reforming of Methanol over Nickel-Based Catalysts for Hydrogen Production. *Biomass and Bioenergy* **2017**, *106*, 29–37.

Graphical abstract:

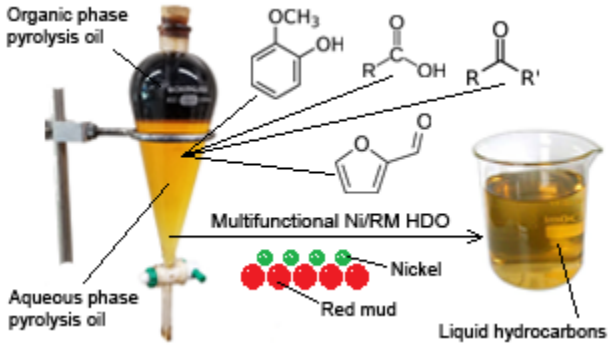

Table of content: